Eye (2021) 35:4–16
https://doi.org/10.1038/s41433-020-01151-z

The ROYAL COLLEGE of OPHTHALMOLOGISTS

ARTICLE

Swept-source optical coherence tomography angiography findings in choroidal and retinal tumors

Ahmet Kaan Gündüz[1,2] · Ibadulla Mirzayev[1] · Rukiye Kasimoglu[1] · Funda Seher Özalp Ateş[3]

Received: 17 July 2020 / Revised: 13 August 2020 / Accepted: 14 August 2020 / Published online: 7 September 2020

Abstract

Objectives To report the swept-source optical coherence tomography angiography (SS-OCTA) findings in choroidal and retinal tumors.

Methods A retrospective noncomparative interventional case series of 60 eyes having various choroidal and retinal tumors imaged with SS-OCTA (Topcon DR1 Triton Plus, Tokyo, Japan) between September 2018 and February 2020 was conducted. Inclusion criteria were tumor thickness <4 mm, tumor base diameter <10 mm, and tumor location at the posterior pole.

Results Choroidal nevi usually demonstrated well-defined borders, hyperreflective internal structure, and no outer retinal involvement on SS-OCTA. Choroidal melanoma, in contrast to nevi, usually had ill-defined borders ($p = 0.018$), mixed hyperreflective–hyporeflective or hyperreflective internal structure ($p = 0.014$), and demonstrated outer retinal involvement ($p < 0.001$). Circumscribed choroidal hemangioma usually presented with well-defined borders, a hyperreflective internal tumor structure with multiple dilated interconnected tumor vessels intermixed with signal void areas representing connective tissue. Optic disc melanocytomas showed a hyporeflective plexus related to blocking of signal by the pigment and an intact radial peripapillary capillary network. There was flow on the surface and slightly deeper within the lesion on B-scan angiography overlay. Retinal astrocytic hamartomas had well-defined borders and a hyperreflective vascular plexus in the superficial and deep retina. Outer retina and choriocapillaris showed hyporeflective change due to shadowing/masking from calcium or high blood flow in the lesion.

Conclusions Each of the different retinal and choroidal tumors studied in this series presented with different SS-OCTA features to aid in the differential diagnosis of these conditions. Good quality images are obtained in patients with good fixation and tumors <3 mm in thickness located at the posterior pole.

Introduction

Due to the longer wavelength (1050 nm) employed and high scan speeds, swept-source optical coherence tomography (SS-OCT) achieves greater tissue penetration and allows better visualization of the internal configuration of the tumors compared to spectral-domain (SD) OCT systems [1, 2]. In addition, SS-OCT provides complementary information such as intraretinal edema, subretinal fluid, photoreceptor atrophy, and retinal pigment epithelium (RPE) atrophy or detachment and can also be used in assessing the dimensions of the lesion in small tumors. SS-OCT angiography (SS-OCTA) devices are the latest OCT technology to become available. These units feature scan rates of 100.000 A-scan/s or higher depending on the machine characteristics [3].

SS-OCTA images are created by computing the differences between SS-OCT B scans consecutively acquired from the same retinal location [4]. The contrast in an SS-OCTA image is generated by movement of the erythrocytes; however, if the velocity of the erythrocytes in the

Supplementary information The online version of this article (https://doi.org/10.1038/s41433-020-01151-z) contains supplementary material, which is available to authorized users.

✉ Ahmet Kaan Gündüz
drkaangunduz@gmail.com

[1] Department of Ophthalmology, Ankara University Faculty of Medicine, Ankara, Turkey

[2] Private Eye Clinic, Ankara, Turkey

[3] Department of Biostatistics, Ankara University Faculty of Medicine, Ankara, Turkey

vessels is very slow, then the consecutively acquired SS-OCT B scans will not be sufficiently different for erythrocyte motion to be detected. Thus, SS-OCTA systems have a characteristic "slowest detectable flow" below which erythrocyte flows cannot be detected [5]. The slowest detectable flow is dependent on the interscan time that is the time between repeated B scans. Therefore, if the interscan time is less, there will be less nonflow artifacts.

SS-OCTA is a noninvasive, dyeless procedure and alongside other indications can also be used to analyze the vascular features of retinal and choroidal lesions located at and posterior to the vascular arcades. In this study, we evaluated the SS-OCTA findings in a variety of choroidal and retinal tumors. In addition, we compared the SS-OCTA features in choroidal nevus (CN) versus (vs) choroidal melanoma (CM).

Materials and methods

The study was designed as a retrospective noncomparative interventional case series of 60 eyes with various choroidal and retinal tumors imaged with SS-OCT and SS-OCTA (Topcon DR1 Triton Plus, Tokyo, Japan) between September 2018 and February 2020. Eyes with choroidal and retinal tumors including CN, CM, choroidal freckle, circumscribed choroidal hemangioma (CCH), choroidal metastatic cancer, optic disc melanocytoma (ODM), retinal astrocytic hamartoma (RAH), and congenital hypertrophy of the retinal pigment epithelium (CHRPE) were included. The study was conducted according to the tenets of the Helsinki Declaration and approved by the Ethics Committee of Ankara University, Faculty of Medicine (Approval number: İ6-387-20).

Inclusion criteria were patient age >18 years, tumor located at the posterior pole or slightly outside of the vascular arcade, tumor thickness <4 mm, and tumor base diameter <10 mm. SS-OCTA images were obtained with 4.5 × 4.5, 6 × 6, 9 × 9, or 12 × 12 mm scans depending on the location of the lesion. SS-OCTA images of poor quality defined as signal strength under 40 (according to the OCT manufacturer's guidelines) and/or image artifact obscuring more than ¼ of the image scan were excluded. Eyes with uveitic or vitreoretinal diseases, previous intraocular surgery except cataract surgery, and high myopia were also excluded. The electronic records of the patients conforming to the above criteria were retrospectively reviewed.

Multimodal imaging with color fundus photography, fundus autofluorescence (AF), SS-OCT, and fluorescein angiography (in selected cases) were also performed using Triton Plus machine. For SS-OCT imaging, 6, 9, or 12 mm scans were employed. A- and B-mode ultrasonography were done using Ellex Eye Cubed device (Mawson Lakes, Australia).

Tumor base diameter and thickness were measured using indirect ophthalmoscopy and A/B-mode ultrasonography. Tumor features noted on B-mode ultrasonography (using 10 MHz probe) were tumor shape, acoustic hollowness/solidity, and presence of subretinal fluid. Fundus AF findings were classified as hypoAF, isoAF, pinpoint hyperAF, patchy hyperAF, and diffuse hyperAF. Tumor features evaluated on SS-OCT included tumor shape (dome vs. plateau vs. flat vs. lumpy–bumpy), tumor reflectivity at the respective retinal/choroidal slab, choroidal shadowing, choroidal vascular structures (compression vs. expansion vs. minimal/no change), and retinal features (drusen, RPE and/or outer retinal atrophy, RPE detachment, subretinal fluid, hyperreflective dots in and under the neurosensory retina, and intraretinal edema).

Tumor features noted on SS-OCTA included tumor margins (well-defined vs. ill-defined), internal reflectivity (hyperreflective vs. isoreflective vs. hyporeflective vs. mixed hypo-hyperreflective), outer retinal slab involvement (absent vs. present), choriocapillaris (CC) vascular features (present vs. compressed/obliterated), intrinsic tumor vessels (visible vs. not visible), and the presence of choroidal neovascularization (CNV) overlying the tumor (present vs. absent). Analysis of en face OCT images available in the OCTA module were not attempted for purposes of this study. Only structural and B-scan OCTA images were evaluated.

The automated segmentation used in the Triton device defines the en face slab for the superficial retinal layer to extend from 2.6 μ beneath the internal limiting membrane to 15.6 μ beneath the interface of inner plexiform layer (IPL) and inner nuclear layer (INL). The deep retinal layer (DRL) slab is generated from 15.6 μ beneath the IPL/INL to 70.2 μ beneath IPL/INL. The outer retina (OR) is segmented 70.2 μ below the IPL/INL border to Bruch's membrane (BM). The CC is segmented from BM to 10.4 μ below BM. The slab thicknesses can be changed to reveal the tumor features in the area of interest. For juxtapapillary tumors or those overhanging the optic disc, SS-OCTA scans centered on the optic disc were used. The automated segmentation layers in the optic disc imaging mode were nerve head, vitreous, radial peripapillary capillary (RPC) plexus, and choroid/disc.

Pearson chi-square/Fisher's exact test was used to analyze the differences between CN and CM in statistical analysis unless otherwise stated.

Results

The study population consisted of 60 patients with 60 eyes having various choroidal and retinal tumors including 14 with CN (Fig. 1a), 12 with CM (Fig. 1i, q), 2 with choroidal

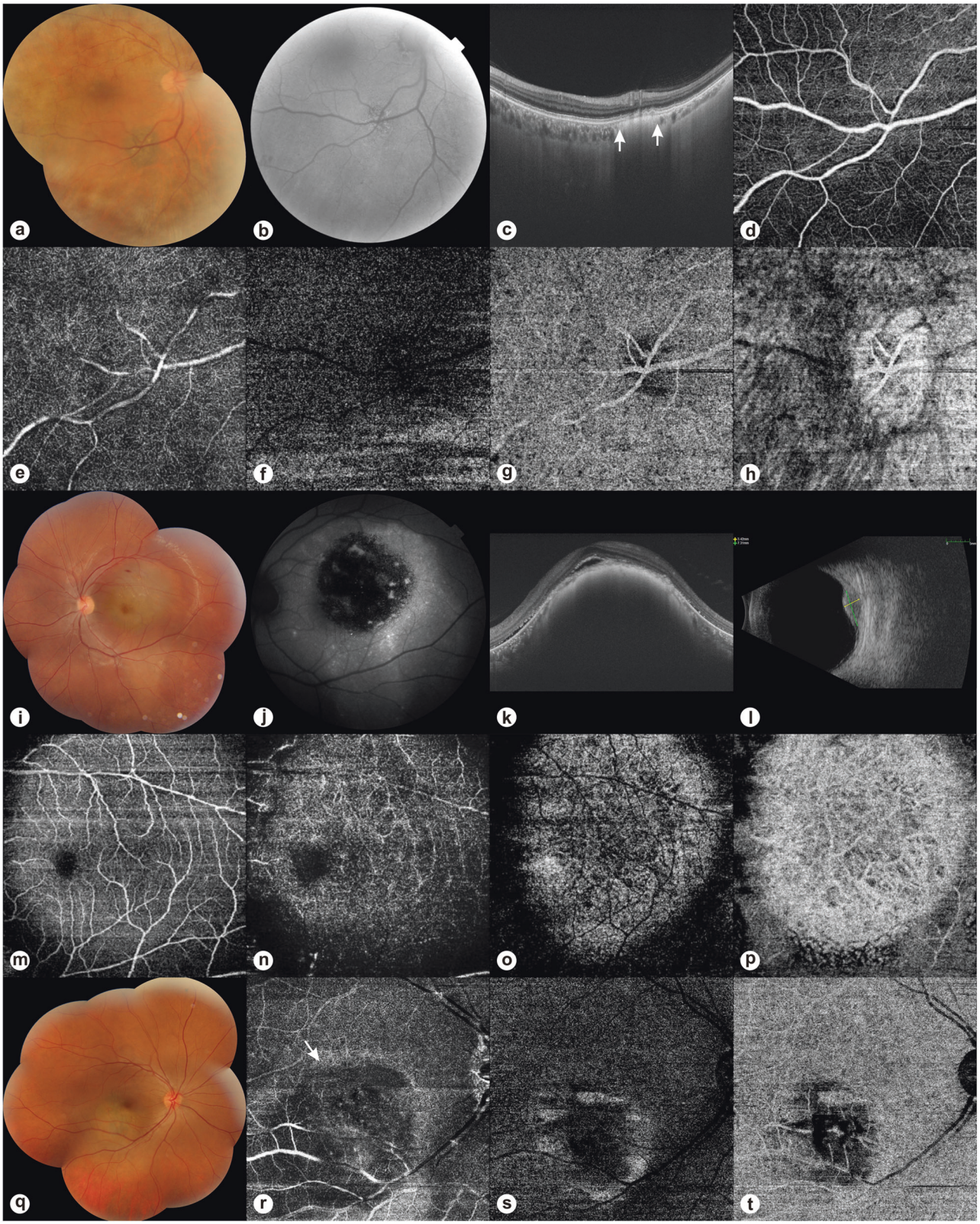

freckle (Fig. 2a), 20 with CCH (Fig. 2i, q), 2 with choroidal metastatic cancer (Fig. 3a), 5 with ODM (Fig. 3i), 3 with RAH (Fig. 4a), and 2 with CHRPE (Fig. 4i). Tumor features, ultrasonography, and fundus AF findings in 60 eyes with choroidal and retinal tumors are depicted in Supplementary Table S1. Many CM (Fig. 1l) had

◀ **Fig. 1 Multimodal imaging including swept-source optical coherence tomography angiography (SS-OCTA) for choroidal nevus (CN) and two cases of choroidal melanoma (CM). a** Color composite photograph of CN with well-defined borders and overlying drusen located along the inferior vascular arcade. The fundus view is hazy due to dense asteroid hyalosis. **b** Fundus autofluorescence (AF) shows pinpoint AF overlying the lesion. **c** Swept-source optical coherence tomography (SS-OCT) (12 mm scan) shows high reflectivity of the CN (arrows), posterior shadowing, and multiple drusenoid retinal pigment epithelial detachments overlying the tumor. **d–h** SS-OCTA (6 × 6 mm scan) demonstrates no change in the superficial retinal plexus (**d**), deep retinal plexus (**e**), outer retina (**f**), and a hyporeflective change in choriocapillaris (**g**). When the choriocapillaris slab is deepened to 150 µm, the hyperreflective plexus of CN becomes visible (**h**). **i** Color composite photograph of a partially pigmented macular CM. **j** Fundus AF shows patchy hyperAF. **k** SS-OCT (12 mm scan) shows CM with dome-shape and high reflectivity, choriocapillaris compression, subretinal fluid, and subretinal lipofuscin. **l** B-mode ultrasonogram depicts a dome-shaped tumor with a largest basal diameter of 7.3 mm and thickness of 3.4 mm with acoustic hollowness. **m–p** SS-OCTA (6 × 6 mm scan) demonstrates no change in the superficial retinal plexus (**m**) and deep retinal plexus (**n**). A hyperreflective plexus is visible in the outer retina (**o**) and choriocapillaris (**p**). Intrinsic tumor vessels of relatively staight caliber with anastomosis are seen in the choriocapillaris slab. **q** Color composite photograph of another partially pigmented CM with a thickness of 3.1 mm. **r**, **s** On SS-OCTA images (9 × 9 mm scan), pressure-induced flow changes (arrow) are visible in the deep retinal plexus (**r**). There is a mixed hypo-hyperreflective tumor plexus in the outer retina (**s**) and choriocapillaris (**t**).

acoustically hollow appearance on B-mode ultrasonography while CN, some CMs, choroidal metastatic lesions (Fig. 3d), CCHs (Fig. 2l), and RAHs (Fig. 4d) were acoustically solid. Choroidal freckles and CHRPE lesions were flat and non measurable on B-mode ultrasonography.

Many CN demonstrated pinpoint hyperAF (Fig. 1b) while the rest of CN and choroidal freckles were isoAF (Fig. 2b). CMs showed either patchy or diffuse hyperAF (Fig. 1j). CCHs demonstrated patchy, diffuse, or pinpoint hyperAF or were isoAF (Fig. 2j). Choroidal metastases demonstrated patchy hyperAF (Fig. 3b). ODM (Fig. 3j) and CHRPE (Fig. 4j) lesions were hypoAF while RAHs demonstrated slight diffuse hyperAF (Fig. 4b).

SS-OCT and SS-OCTA features are given in Supplementary Table S2 and Table 1 respectively. SS-OCT findings included tumor shape, tumor reflectivity, choroidal shadowing, choroidal vascular features, and retinal changes including drusen, RPE and/or outer retinal atrophy, RPE detachment, subretinal fluid, lipofuscin deposits, and intraretinal edema. Many tumors including CN, CMs (Fig. 1k), and CCHs (Fig. 2k, r) had dome-shaped appearance. Some CN had plateau (Fig. 1c) contour while choroidal freckles (Fig. 2c) and CHRPEs (Fig. 4k) displayed flat appearance. Choroidal metastases featured a lumpy–bumpy configuration (Fig. 3c). RAHs had dome (Fig. 4c) or flat contour and ODMs had dome shape (Fig. 3k). Tumor reflectivity was usually medium-high for CN, CM, and choroidal freckle (Figs. 1c, k, 2c), medium for CCH (Fig. 2k, r), and low for choroidal metastasis (Fig. 3c). However, choroidal metastatic lesions usually had additional high reflective interspersed dots, probably representing metastatic tumor foci and/or localized collections of lipofuscin (Fig. 3c). ODM (Fig. 3k), RAH (Fig. 4c), and CHRPE (Fig. 4k) had medium to high reflectivity on SS-OCT. Choroidal shadowing was seen in almost all choroidal and retinal tumors and was more intense with heavily pigmented tumors and those having calcium. On SS-OCT, CN (Fig. 1c) and CM (Fig. 1k) showed compression of choroidal vascular features. Two deeply located CN, choroidal freckles, and retinal tumors displayed minimal compromise of CC and choroidal vascular features (Fig. 2c). CCHs (Fig. 2k, r) and choroidal metastases (Fig. 3c) usually resulted in expansion of choroidal vasculature.

On SS-OCT, commonly seen retinal features included drusen, RPE and/or outer retinal atrophy, and RPE detachments for CN (Fig. 1c); RPE and/or outer retinal atrophy, subretinal fluid, and sub- and intraretinal lipofuscin deposits for CM (Fig. 1k); subretinal fluid and intraretinal edema sometimes with retinal schisis for CCH (Fig. 2k, r); RPE and/or outer retinal atrophy, subretinal fluid, and sub- and intraretinal hyperreflective dots for choroidal metastasis (Fig. 3c); multiple hyperreflective dots representative of heavily pigmented cell collections for ODM (Fig. 3k); nerve fiber layer origin, optically empty (moth-eaten) spaces, and vitreoretinal traction for RAH (Fig. 4c); and, nodularity of the RPE and outer retinal atrophy for CHRPE (Fig. 4k). Choroidal freckles had no significant overlying retinal changes.

SS-OCTA features evaluated in this study included tumor margins, internal reflectivity, outer retinal involvement, CC status, intrinsic tumor vessels, and presence of CNV. CN usually demonstrated well-defined borders and hyperreflective internal structure on SS-OCTA (Fig. 1d–g). Extensive fibrosis and drusen over the lesion were associated with a hyporeflective appearance in the CC slab in two eyes (Fig. 1g). When the slab thickness was increased to deeper choroid levels, these CN were visible as a hyperreflective plexus (Fig. 1h). Outer retinal involvement was noted in only 2 of 14 (14.3%) CN with overlying RPE atrophy/RPE detachment. Intrinsic tumor vessels were not visible in any CN.

CMs, in contrast to CN, usually had ill-defined borders, mixed hyperreflective–hyporeflective or hyperreflective internal structure, and demonstrated outer retinal involvement (Fig. 1m–p, r–t). Two CMs with thickness >3 mm producing bowing of the RPE and neurosensory retina also manifested with pressure-induced flow changes in the superficial and deep retinal

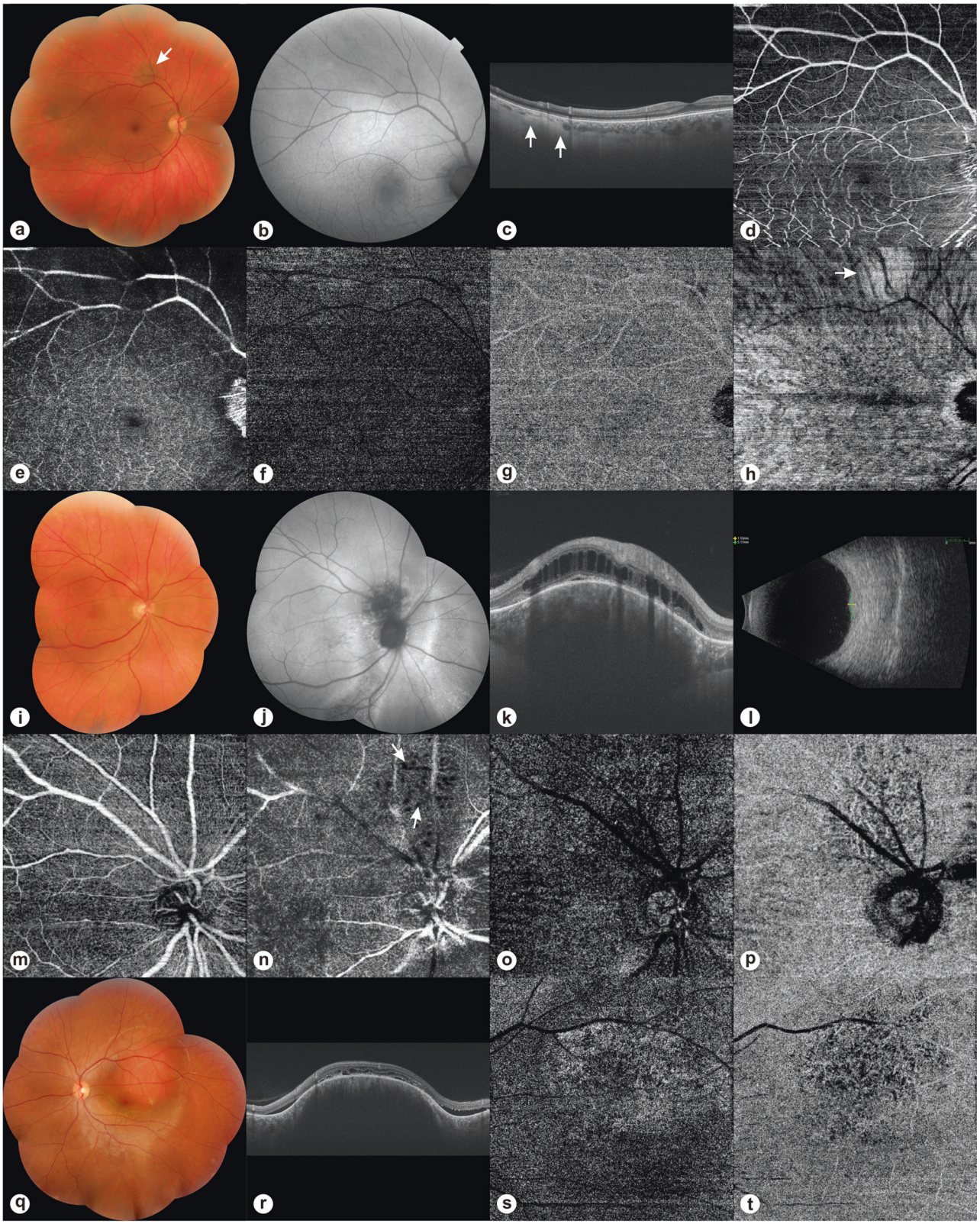

slabs (Fig. 1q, r). Internal tumor vessels were not visible in the nine pigmented tumors but were discernible in the three partially pigmented tumors (Fig. 1m–p). In these three eyes with partially pigmented CMs, intratumoral vessels had a relatively straight appearance with anastomosis and crosslinks.

◀ **Fig. 2 Multimodal imaging including swept-source optical coherence tomography angiography (SS-OCTA) for choroidal freckle and two cases of circumscribed choroidal hemangioma (CCH).** **a** Color composite photograph of choroidal freckle with ill-defined irregular borders located above the superior vascular arcade (arrow). **b** Fundus autofluorescence (AF) shows an isoAF lesion. **c** Swept-source optical coherence tomography (SS-OCT) (12 mm scan) shows a flat lesion with medium reflectivity, posterior choroidal shadowing (arrows), and preservation of choriocapillaris and superficial choroidal vessels. **d–h** SS-OCTA (9 × 9 mm scan) demonstrates no change in the superficial retinal plexus (**d**), deep retinal plexus (**e**), outer retina (**f**), and choriocapillaris (**g**). A well-defined deep-seated hyperreflective network in the choroid layer visible at 170 µm beneath the Bruch's membrane (arrow) (**h**). **i** Color composite photograph of CCH located superior to the optic disc. **j** Fundus AF shows a predominantly hypoAF lesion with areas of pinpoint hyperAF. There are also some retinal pigment epithelial (RPE) and AF changes from prior subretinal fluid inferior to the optic disc. **k** SS-OCT (6 mm scan) shows dome-shaped medium reflective CCH, posterior shadowing, intraretinal schisis, and minor subretinal fluid. **l** B-mode ultrasonogram displays an acoustically solid tumor with a thickness of 1.5 mm and largest basal diameter of 5.2 mm. **m–p** 6 × 6 mm SS-OCTA scans depict normal superficial retinal plexus (**m**), flow void areas from intraretinal schisis in the deep retinal plexus (arrows) (**n**), and normal outer retina (**o**). Intermingled club-shaped anastamosing intratumoral vessels are visible in the choriocapillaris layer (**p**). **q** Color composite photograph of another CCH with a thickness of 2.9 mm located in the posterior pole. **r** SS-OCT (12 mm scan) shows dome-shaped medium reflective CCH, posterior shadowing, RPE atrophy, and subretinal fluid. **s**, **t** SS-OCTA (9 × 9 mm scan) demonstrates outer retinal involvement due to unmasking of flow in intratumoral vessels from RPE atrophy (**s**) and irregularly shaped intratumor vessels in the choriocapillaris layer (**t**).

Statistical comparison of CN and CM revealed that two groups had significantly different thicknesses of 1.3 (1.0–2.5) and 2.8 (2.2–3.9) mm, respectively ($p < 0.001$, independent samples t test). With respect to margins, 10 of 14 (71.4%) CN vs. 3 of 12 (25.0%) CMs had well-defined margins ($p = 0.018$). Of 14 CN, 12 (85.7%) had high reflectivity and 2 (14.3%) had surface hypo-, and deep hyperreflectivity. Of 12 CMs, 8 (66.7%) had mixed hypo-hyperreflectivity and 4 (33.3%) had hyperreflectivity. The difference between CM and CN with respect to internal reflectivity was statistically significant ($p = 0.014$). Outer retinal involvement was noted in all CMs and in only 2 of 14 (14.3%) CN with overlying RPE atrophy/RPE detachment ($p < 0.001$). CC was compressed/infiltrated by tumor in 12 of 14 CN and in all CMs ($p = 0.173$). Intrinsic tumors were present in 3 of 12 (25.0%) CMs demonstrating light-moderate pigmentation and in none of CN ($p = 0.085$, slightly significant).

Choroidal freckles displayed no change in the superficial and deep retinal plexi, outer retina, and CC slabs on SS-OCTA (Fig. 2d–g). There was a well-defined deep-seated hyperreflective network in the choroid layer in the 2 cases studied using SS-OCTA (Fig. 2h).

CCHs usually presented with well-defined borders, a hyperreflective internal tumor with multiple dilated interconnected club-shaped tumor vessels intermixed with signal void areas, the latter probably representing the intervening connective tissue portions of the tumor on SS-OCTA. There was no change in the superficial and outer retina but many cases having intraretinal schisis/cystoid edema presented with flow void changes in the DRL (Fig. 2m–o). Two CCHs with thickness >3 mm produced pressure vascular changes in the DRL similar to CMs (Fig 1q, r). Internal tumor vessels were present in the CC slab in all CCHs (Fig. 2p, t). Additionally, four CCHs >2 mm in thickness associated with RPE atrophy also demonstrated outer retinal involvement due to unmasking of flow in intratumoral vessels (Fig. 2q, s).

On SS-OCTA, choroidal metastasis from breast carcinoma had ill-defined borders and a hyporeflective internal tumor structure often admixed with hyperreflective areas, probably presenting stromal and vascular portions of the tumor respectively (Fig. 3e–g). A disorganized choroidal plexus with thick and fine vessels, large avascular zones, vascular loops, and anastomosis were seen in our two cases with breast cancer metastasis to the choroid (Fig. 3h). There were flow void artifacts from subretinal fluid in the DRL and unmasking artifacts from RPE atrophy in the outer retinal slab (Fig. 3f, g).

ODMs showed a hyporeflective plexus related to blocking of signal by the pigment and an intact RPC network on SS-OCTA (Fig. 3m–p). There was flow on the surface and slightly deeper within the lesion on B-scan angiography overlay (Fig. 3l). Of three RAHs, one had a juxtapapillary location and the other two were located in the macular area. RAHs had well-defined borders, a hyperreflective internal tumor structure, and fine branching tumor vessels. Superficial and deep retina showed tumor vascular network (Fig. 4e, f). Outer retina and CC showed hyporeflective change due to shadowing/masking from calcium or high blood flow in the retinal lesion (Fig. 4g, h). Moth-eaten cavities within the lesion presented as nonflow areas in the DRL with projection artifacts in the outer retina and CC (Fig. 4f, h). CHRPE cases demonstrated well-defined borders, a hyperreflective plexus in the superficial and DRLs (Fig. 4m, n). There were flow signals in the overlying retina on B-scan angiography overlay (Fig. 4l). Masking of the outer retina and CC (Fig. 4o, p) led to signal void areas. Internal tumor vessels were not visible in ODM and CHRPE.

None of the choroidal and retinal lesions was associated with CNV in this series. Tumors >3 mm in thickness and those associated with overlying bullous subretinal fluid were difficult to image on the SS-OCTA platform although occasionally macular tumors with thicknesses >3 mm and <4 mm could be imaged satisfactorily. Patient attentiveness, cooperation, and motivation were also important factors in obtaining good quality scans. Several scans were excluded

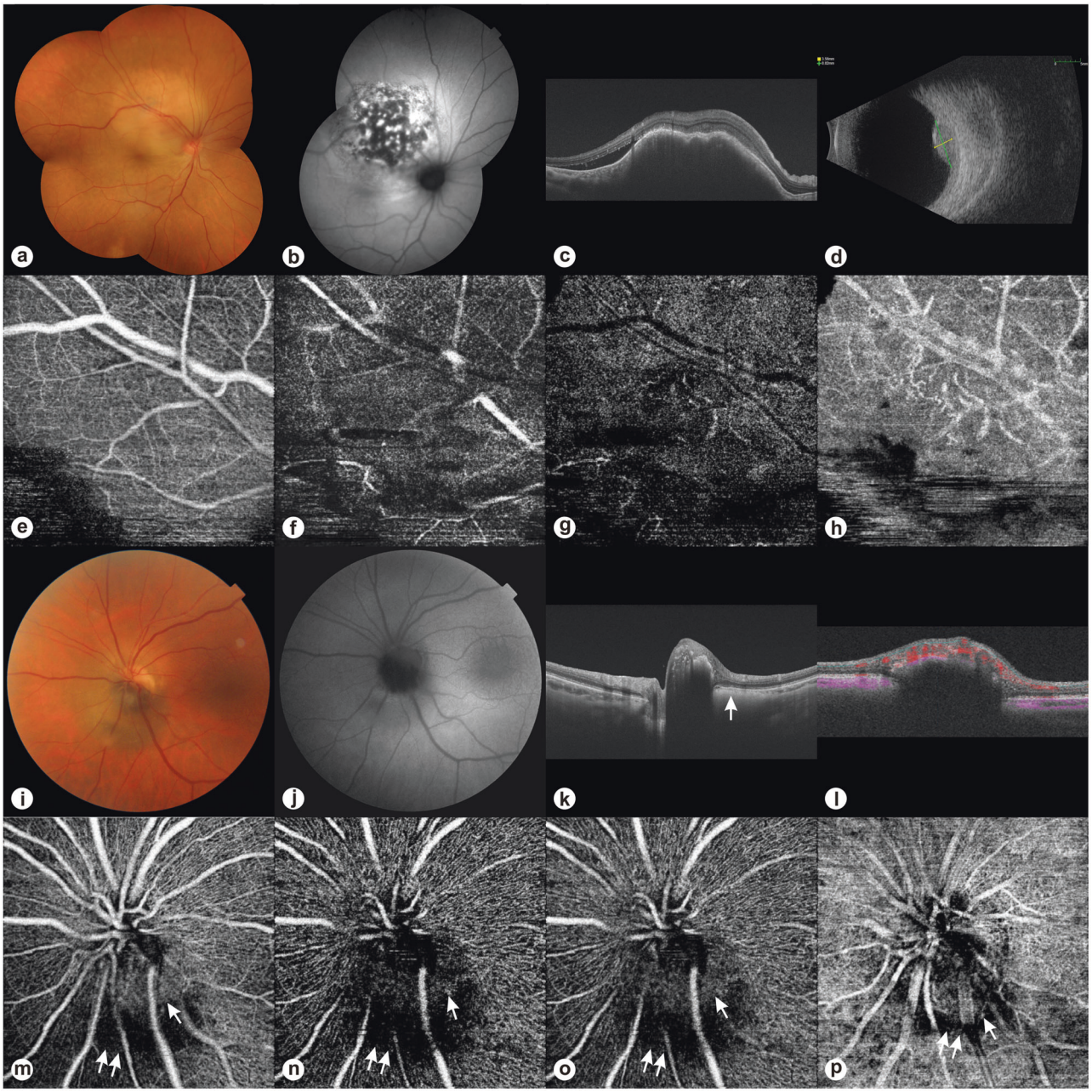

Fig. 3 Multimodal imaging including swept-source optical coherence tomography angiography (SS-OCTA) for choroidal metastasis from breast cancer and optic disc melanocytoma (ODM). a Color composite photograph of juxtapapillary choroidal metastasis from breast cancer. **b** Fundus autofluorescence (AF) shows patchy hyperAF. **c** Swept-source optical coherence tomography (SS-OCT) (12 mm scan) shows a lumpy–bumpy contour, low reflectivity, subretinal fluid, and interspersed high reflective dots. **d** B-mode ultrasonogram shows an acoustically solid tumor with a thickness of 3.6 mm and largest basal diameter of 8.8 mm. **e–h** SS-OCTA (6 × 6 mm) displays no change in the superficial retinal plexus (**e**), flow void artifacts from subretinal fluid in the deep retinal plexus (**f**), and unmasking artifacts from retinal pigment epithelial atrophy in the outer retina (**g**). There is a disorganized plexus with thick and fine vessels, vascular loops, and anastomosis in the choriocapillaris (**h**). Segmentation and motion artifacts are visible in the lower ¼ part of the SS-OCTA images at all segmentation layers. **i** Color fundus photograph of ODM overhanging the optic disc. **j** Fundus AF shows a hypoAF lesion. **k** SS-OCT (12 mm scan) demonstrates a dome-shape contour to the mass, medium reflectivity, multiple hyperreflective dots overlying the lesion, and choroidal shadowing due to the choroidal component of ODM (arrow). **l** B-scan angiography overlay shows flow (depicted in red) on the surface and slightly deeper within the lesion. **m–p** SS-OCTA optic disc images (4.5 × 4.5 mm) show tumor vessels at various levels (arrows), an intact RPC network, and hyporeflectivity related to blocking of signal by the pigment (double arrows) at automated segmentation levels of nerve head (**m**), vitreous (**n**), radial peripapillary capillary (RPC) (**o**), and choroid/disc (**p**).

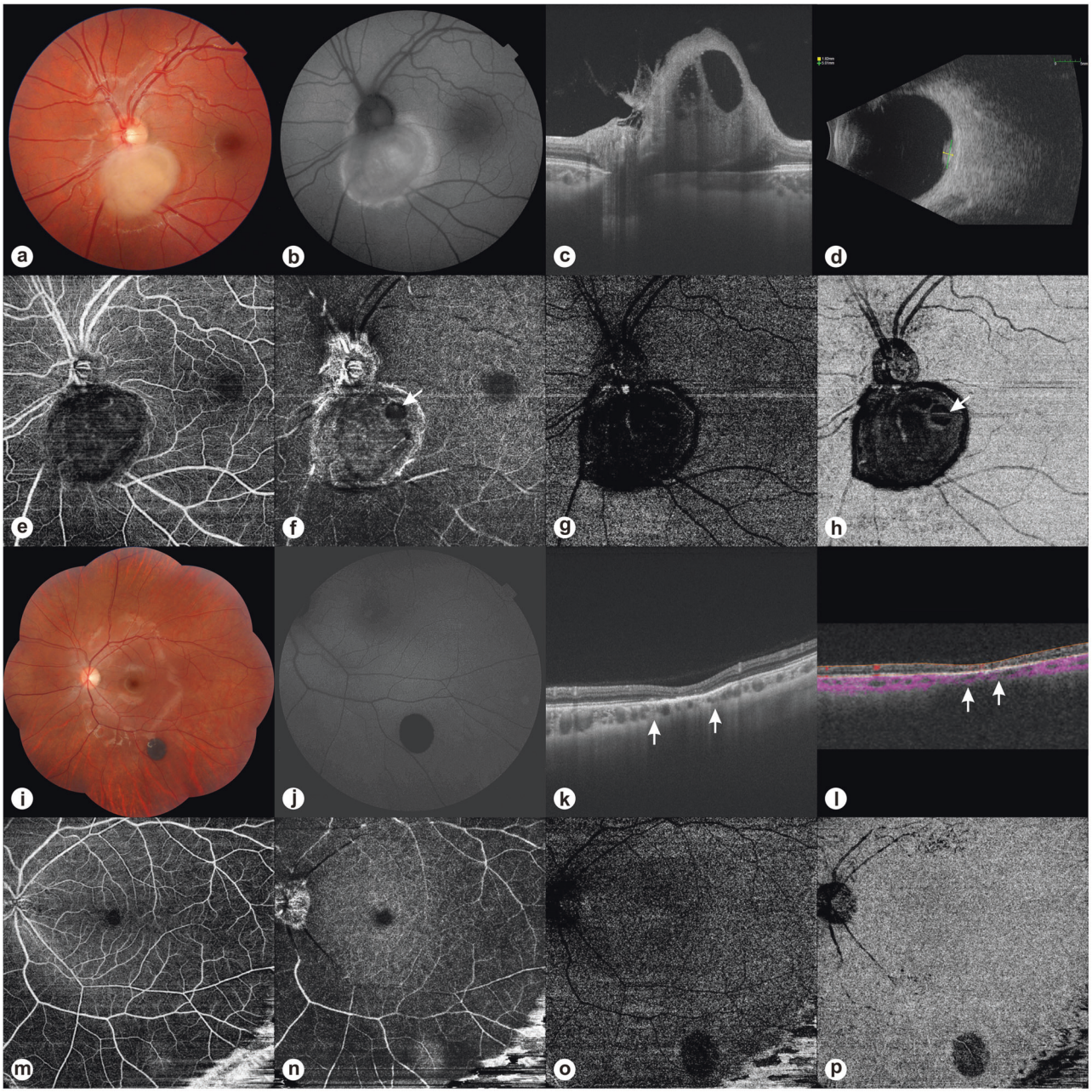

Fig. 4 Multimodal imaging including swept-source optical coherence tomography angiography (SS-OCTA) for retinal astrocytic hamartoma (RAH) and congenital hypertrophy of the retinal pigment epithelium (CHRPE). a Color fundus photograph of juxtapapillary RAH. **b** Fundus autofluorescence (AF) shows diffuse slight hyperAF in the lesion. **c** Swept-source optical coherence tomography (SS-OCT) (12 mm scan) features include dome-shape contour, medium reflectivity, moth-eaten cavities, and vitreoretinal traction. **d** B-mode ultrasonogram shows an acoustically solid tumor with a largest basal diameter of 5.0 mm and thickness of 1.8 mm. **e–h** 9 × 9 mm SS-OCTA images show tumor vascular network in the superficial retinal plexus (**e**) and more prominently in the deep retinal plexus (**f**). There is flow void corresponding to the cavitation in the tumor (arrow) (**f**). There is hyporeflective change due to shadowing/masking from calcium or high blood flow in the retinal lesion in the outer retina (**g**) and choriocapillaris (**h**). Projection artifact of the moth-eaten cavities are visible in the choriocapillaris slab (arrow) (**h**). **i** Color composite photograph of CHRPE located inferior to the inferior arcade. **j** Fundus AF shows a hypoAF lesion. **k** SS-OCT (12 mm scan) demonstrates a highly reflective flat lesion (arrows), focal retinal pigment epithelium hyperplasia, and outer retinal atrophy. **l** Retinal flow signals (shown in red) over the tumor (arrows) are evident on the B-scan angiography overlay. **m–p** SS-OCTA (12 × 12 mm scan) demonstrates hyperreflective plexus in the superficial (**m**) and in the deep (**n**) retinal layers, more prominent in the latter. There is masking of the outer retina (**o**) and choriocapillaris (**p**) by pigment leading to signal void areas. Out-of-window artifacts are visible in the right lower corner of the SS-OCTA images.

Table 1 Swept-source optical coherence tomography angiography features in 60 eyes with choroidal and retinal tumors.

SS-OCTA features	Chor nevus ($n = 14$)	Chor mel ($n = 12$)	Chor freckle ($n = 2$)	CCH ($n = 20$)	Chor Mets ($n = 2$)	ODM ($n = 5$)	RAH ($n = 3$)	CHRPE ($n = 2$)
Tumor margins								
Well-defined	10	3	2	18	–	–	3	2
Ill-defined	4	9	–	2	2	5	–	–
Internal reflectivity[a]								
Hyperreflective	12	4	2	20	–	5	3	–
Hyporeflective	–	–	–	–	–	–	–	2
Mixed hyper-hyporeflective	–	8	–	–	2	–	–	–
Surface hypo-, deeper hyperreflective	2	–	–	–	–	–	–	–
Outer retinal involvement						N/A		
Present	2	12	–	4	–		–	2
Absent	12	–	2	16	2		3	–
Choriocapillaris								
Present	2	–	2	20	–	2	3	2
Compressed/infiltrated by tumor	12	12	–	–	2	3[b]	–	–
Intrinsic tumor vessels								
Visible	–	3	–	20	2	–	2	–
Not visible	14	9	2	–	–	5	1	2
CNV								
Present	–	–	–	–	–	–	–	–
Absent	14	12	2	20	2	5	3	2

SS-OCTA swept-source optical coherence tomography angiography, *Chor* choroidal, *Mel* melanoma, *Mets* metastasis, *CCH* circumscribed choroidal hemangioma, *ODM* optic disc melanocytoma, *RAH* retinal astrocytic hamartoma, *CHRPE* congenital hypertrophy of the retinal pigment epithelium, *CNV* choroidal neovascularization, *N/A* not available, could not be evaluated.

[a]At the respective retinal/choroidal slab.

[b]Due to the choroidal component of ODM.

because of image artifacts and poor quality images due to poor patient fixation.

Discussion

Choroidal nevus, melanoma, and freckle

CN is the most common benign intraocular tumor in adults with an expected frequency of 6% in the Caucasian population [6]. On SS-OCT, CN usually manifested with dome/plateau shape, high reflectivity, choroidal shadowing, RPE and/or outer retinal atrophy, drusen, and RPE detachment. On SS-OCTA, CN usually presented with well-defined borders. Superficial, deep, and outer retina were usually not involved. Outer retinal involvement was noted in only two eyes with CN, one with overlying RPE atrophy and one with RPE detachment. The major change was in the CC-choroid slab and CN manifested as a hyporeflective to hyperreflective plexus. CN was generally hyperreflective but extensive drusen and fibrosis overlying the lesion probably led to vascular disruption and a hyporeflective change in the CC, as previously reported [7]. For deeper seated CN, CC in the standard slab thickness may look normal. However, when the CC slab is adjusted to include the deeper choroid, the hyperreflective plexus of CN is noted. Choroid images may vary between different OCTA platforms. Cennamo et al. reported no changes in CC in 60 eyes with CN using SD-OCTA [8]. There was no CNV associated with CN detectable on SS-OCTA in our study.

CM is the most frequent intraocular malignant tumor in adults. The tumor has a predilection for whites [9]. On SS-OCT, CMs presented with dome shape, high reflectivity, choroidal shadowing, compression of CC, subretinal fluid, and intraretinal/subretinal lipofuscin. On SS-OCTA, CMs usually had ill-defined borders, mixed hyperreflective–hyporeflective or hyperreflective internal structure, and demonstrated outer retinal involvement. The outer retinal involvement may be due to unmasking of tumor vascular patterns in the CC and choroid from RPE and/or outer retinal atrophy. The mixed reflectivity (hyper on the outer rim and hypo in the middle) may represent areas of intense lipofuscin or melanin content manifesting as hyporeflective change in the center while the more peripheral vascular portions as hyperreflective change [7, 10]. Garcia-Arumi et al. [11] speculated that the hyperreflective

appearance in CN may be due to the reflectance of OCT light and the hyporeflective appearance in CM due to signal blockage.

In our study, there are statistically important differences between CN and CM with respect to tumor margins, tumor reflectivity, and outer retinal involvement on SS-OCTA. Therefore, SS-OCTA can be used to differentiate CM vs. CN alongside other multimodal imaging methods [11]. Intrinsic tumor vessels were visible only in partially pigmented CM and not in heavily pigmented CM and CN on SS-OCTA in our study. Similar results have also previously been demonstrated using SD-OCTA [12]. Garcia-Arumi et al. found that 45% of CMs displayed abnormal vasculature such as loops and thick vessels within the tumor [11]. Pellegrini et al. reported that Zeiss Elite Plex SS-OCTA disclosed the intrinsic microvasculature in all of the 22 CMs with varying tumor base diameter, thickness, and location evaluated in their study [13]. Therefore SS-OCTA systems with a greater scan depth may show intrinsic tumor vasculature better in thicker tumors.

Valverde-Megias et al. evaluated macular changes remote from the tumor in eyes having CN and CM with SD-OCTA [14]. They found that compared with the contralateral healthy eye, eyes with CN demonstrate similar central macular thickness (CMT), foveal avascular zone (FAZ), and capillary vascular density (CVD) [14]. In contrast, eyes with CM show increased CMT, enlarged FAZ, and reduced CVD compared to the contralateral healthy eye [14].

Choroidal freckle is defined as a choroidal melanocytic lesion not causing disturbance in the overlying choroid so that choroidal vessels are visible ophthalmoscopically. SS-OCT of choroidal freckles revealed no retinal and CC involvement and a deep-seated flat tumor in the choroid layer. Choroidal freckles displayed no change in the superficial, deep, and outer retina and CC on SS-OCTA [7]. There was a well-defined deep-seated hyperreflective network in the choroid layer in the two cases studied using SS-OCTA. Internal tumor vessels were not visible in choroidal freckles similar to CN.

Circumscribed choroidal hemangioma

CCH is a common uveal vascular tumor generally located in the posterior pole leading to visual loss in patients aged 20–40 years old. On SS-OCT, CCHs manifested as a dome-shaped mass with medium reflectivity, choroidal shadowing, subretinal fluid, intraretinal edema, and intraretinal schisis. In addition, there was expansion of medium and large sized choroidal vessels without compression of CC. On SS-OCTA, CCHs usually presented with well-defined borders, a hyperreflective internal tumor structure featuring intertwined and irregularly organized large-calibre vessels mixed with signal void areas, probably representing connective tissue portions of the tumor. Internal tumor vessels were present in all the cases and have previously been described under a variety of names including "club-shaped", "spaghetti", and "bag of worms" [15, 16]. CCHs usually did not demonstrate retinal involvement except for flow void changes from retinal schisis/edema in the DRL. However, four eyes with long standing CCHs and tumor thickness >2 mm featured RPE atrophy and demonstrated outer retinal involvement due to unmasking of flow in intratumoral vessels.

Choroidal metastatic cancer

Metastatic cancer to the uvea may be the most frequent uveal malignancy in adults. Choroid is affected in 88% of these patients because of its rich vascular supply enabling tumor emboli to sequester. The real frequency of choroidal metastatic cancer is probably underestimated because many choroidal metastases become apparent late in the course of disease and are associated with widespread tumor dissemination and poor prognosis. Breast is the most frequent site (37%) for metastatic cancer to the choroid followed by lung (27%), gastrointestinal system (4%), and the kidney (4%) [17]. On SS-OCT, choroidal metastatic cancer presented with low reflectivity and infiltration of the CC and choroid with hyperreflective dots, the latter probably representing metastatic tumor cells and/or lipofuscin collections. Choroidal metastatic tumors had a lumpy–bumpy contour, displayed subretinal fluid, and sub/intraretinal high reflective spots. On SS-OCTA, choroidal metastasis had ill-defined borders, a hyperreflective internal tumor structure often admixed with hyporeflective areas, probably presenting vascular and stromal portions of the tumor respectively. Hyporeflectivity and lack of blood flow within certain areas of metastatic tumor might also be due to the shadowing artifact of the overlying retinal edema and subretinal fluid as well as due to the high velocity of blood flow within the tumor vasculature (fringe effect) [18]. A disorganized choroidal plexus with thick and fine vessels, large avascular zones, vascular loops, and anastomosis were seen in our two cases with breast cancer metastatic to the choroid [7, 8]. This vasculature pattern was different from the relatively straight vessels seen in less pigmented CMs and intermingled anastomosing vessels observed in CCHs.

Optic disc melanocytoma

ODM is a variant of melanocytic nevus that is classically located on the optic disc. It can also occur in the uvea. ODM is a deeply pigmented lesion usually located on all or part of the optic disc. Unlike uveal melanoma, ODM does not appear to have a predilection for whites.

SS-OCT of ODM showed dome shape, dense posterior shadowing, and multiple hyperreflective dots probably

resulting from heavily pigmented tumor cell collections overlying the lesion continuous with the inner retinal layer. SS-OCT may also be helpful in showing the extent of subretinal fluid and cystoid retinal edema. Only one ODM displayed intraretinal edema on SS-OCT in our series. On SS-OCTA, ODM had ill-defined borders, a hyporeflective internal structure possibly related to blocking of signal by the excess melanin content of ODMs, and an intact RPC network. There was flow on the surface and slightly deeper within the lesion on B-scan angiography overlay. Previous studies also showed fine abnormal retinal vasculature on the surface of the ODM on OCTA [19, 20]. Takkar et al. reported the presence of superficial meshwork of vasculature over the ODM using SS-OCTA [21]. Jain et al. reported OCTA findings including heterogeneously distributed sparse vasculature intrinsic to ODM with a prominent vessel seen in the center of the lesion [22]. OCTA is also useful in showing CNV, a finding associated with ODM in 1% of cases, especially if there is adjacent subretinal exudation, subretinal fluid, and subretinal hemorrhage. OCTA may also be helpful in the detection of branch retinal vein and branch retinal artery occlusion, two vascular occlusive events that may rarely be associated with ODM. The 5 cases of ODM in our study did not manifest CNV or vascular occlusive events.

Retinal astrocytic hamartoma

RAHs usually showed dome shape, thickening of the retinal nerve fiber layer, focal vitreoretinal traction, moth-eaten cavities, and choroid shadowing from intralesional calcium on SS-OCT. There was a dense hyperreflective vascular network within the RAH in the superficial and especially the deep retinal plexi on SS-OCTA. Ill-defined arborizing tumor vessels were visible especially in the deep capillary plexus. Outer retina and CC showed hyporeflective changes due to shadowing/masking from retinal lesion which may be due to calcium and/or high blood flow. However, type IV tumors with cavitation have been reported to display central hyporeflectivity and hyperreflective signals in the lesion periphery possibly representing microvascular flow within the walls of the honeycomb-like mass [23, 24]. Yung et al. reported a central feeder vessel associated with an abnormal vascular plexus in RAH using SD-OCTA [25].

Congenital hypertrophy of the retinal pigment epithelium

CHRPE is typically a pigmented flat lesion with a halo around its margins and lacunae within the lesion. It usually occurs as an unifocal and isolated lesion. In congenital grouped pigmentation of the retina or bear tracks, multiple CHRPE lesions can be seen. This multifocal variant may be associated with familial adenomatous polyposis and Gardner's syndrome.

SS-OCT showed normal inner retina, thinning of outer retina, and thickening of the RPE compared to the adjacent retina. On SS-OCTA, CHRPE lesions demonstrated well-defined borders, a hyperreflective plexus in the superficial and DRLs, corresponding retinal vascular changes on the B-scan overlay, and masking of the outer retina and CC leading to signal void areas [7, 26]. Internal tumor vessels were not visible. Shanmugam et al. found normal retinal OCTA findings over CHRPE while Toledo et al. reported similar findings to our study [7, 26]. Sufficiently large lacunae within CHRPE may reveal normal underlying choroidal vessels.

Image artifacts occur frequently in OCTA images. Commonly seen image artifacts in SS-OCTA include banding, segmentation, motion, unmasking, and blink artifacts [18, 27]. These artifacts occur more frequently in eyes with pathology. At least one type of artifact was present in 89% of the images in eyes having various pathologies on SS-OCTA [27]. In our study, many eyes evaluated during the inclusion period were excluded from analysis because of image artifacts and poor quality images.

In conclusion, the SS-OCTA platform evaluated in this study was useful for the differential diagnosis of various choroidal and retinal tumors. There were significant differences in the SS-OCTA imaging features of CN vs. CM, the two most common choroidal melanocytic lesions encountered in ocular oncology practice. Together with other multimodal imaging techniques, SS-OCTA can be used to establish the diagnosis of many choroidal and retinal tumors located in the posterior pole. Similar findings have previously been reported using SD-OCTA systems [7, 8, 28]. Best results in SS-OCTA imaging are obtained with tumors <3 mm in thickness, small base diameter, and posterior pole location. SS-OCTA requires patient fixation and better technician skills compared to SS-OCT testing. SS-OCTA allows for segmentation of the retina into specific layers which is not possible with conventional dye-based angiography systems [28]. As a noninvasive procedure, SS-OCTA may offer certain advantages over dye-based angiography systems but is currently not a total replacement for these angiography systems because of its limitations in visualizing tumors >4 mm in thickness and with peripheral location.

Summary

What was known before

- There are few reports describing spectral-domain optical coherence tomography angiography (SD-OCTA) and

swept-source optical coherence tomography (SS-OCTA) findings of intraocular tumors. Many published reports are case series and there have been only few publications describing SD-OCTA findings of intraocular tumors on a large scale.

What this study adds

- This study reviews the multimodal imaging features including SS-OCTA in a variety of retinal and choroidal tumors. SS-OCTA, by virtue of its longer wavelength, deep penetration, and high scan speed shows choroidal vascular structures better compared to SD-OCTA systems. This study evaluates the SS-OCTA findings in 60 patients with various choroidal and retinal tumors located at the posterior pole. It highlights several novel previously unreported features of these tumors on SS-OCTA and discusses the limitations of SS-OCTA imaging in this context.

Compliance with ethical standards

Conflict of interest The authors declare that they have no conflict of interest.

Publisher's note Springer Nature remains neutral with regard to jurisdictional claims in published maps and institutional affiliations.

References

1. Filloy A, Caminal JM, Arias L, Jordán S, Català J. Swept source optical coherence tomography imaging of a series of choroidal tumours. Can J Ophthalmol. 2015;50:242–8.
2. Francis JH, Pang CE, Abramson DH, Milman T, Folberg R, Mrejen S, et al. Swept-source optical coherence tomography features of choroidal nevi. Am J Ophthalmol. 2015;159:169–76.
3. Miller AR, Roisman L, Zhang Q, Zheng F, de Oliveira Dias JR, Yehoshua Z, et al. Comparison between spectral-domain and swept-source optical coherence tomography angiographic imaging of choroidal neovascularization. Investig Ophthalmol Vis Sci. 2017;58:1499–505.
4. Tan ACS, Tan GS, Denniston AK, Peane KA, Ang M, Milea D, et al. An overview of the clinical applications of optical coherence tomography angiography. Eye. 2018;32:262–86.
5. de Carlo TE, Romano A, Waheed NK, Duker JS. A review of optical coherence tomography angiography (OCTA). Int J Retina Vitreous. 2015;1:5.
6. Sumich P, Mitchell P, Wang JJ. Choroidal nevi in a white population: the Blue Mountains Eye Study. Arch Ophthalmol. 1998;116:645–50.
7. Toledo JJ, Asencio M, García JR, Morales LA, Tomkinson C, Cajigal C. OCT angiography: imaging of choroidal and retinal tumors. Ophthalmol Retina. 2018;2:613–22.
8. Cennamo G, Romano MR, Breve MA, Velotti N, Reibaldi M, de Crecchio G, et al. Evaluation of choroidal tumors with optical coherence tomography: enhanced depth imaging and OCT-angiography features. Eye. 2017;31:906–15.
9. Shields CL, Sioufi K, Srinivasan A, Di Nicola M, Masooman B, Barna LE, et al. Visual outcome and millimeter incremental risk of metastasis in 1780 patients with small choroidal melanoma managed by plaque radiotherapy. JAMA Ophthalmol. 2018; 136:1325–33.
10. Motiani MV, McCannel CA, McCannel TA. Optical coherence tomography angiography findings in ocular oncology and radiation retinopathy. In: Chow DR, De Oliveira PRC, editors. OCT angiography. India: Thieme; 2018. p. 99–111.
11. Garcia-Arumi Fuste C, Peralta Iturburu F, Garcia-Arumi J. Is optical coherence tomography angiography helpful in the differential diagnosis of choroidal nevus versus melanoma? Eur J Ophthalmol. 2020;30:723–9.
12. Cennamo G. OCT angiography examination of choroidal nevi and melanomas. In: Lumbroso B, Huang D, Chen CJ, Jia Y, Rispoli M, Romano A, Waheed NK, editors. Clinical OCT angiography Atlas. Philadelphia, PA, USA: Jaypee Brothers; 2015. p. 151–5.
13. Pellegrini M, Corvi F, Invernizzi A, Ravera V, Cereda MG, Staurenghi G. Swept-source optical coherence tomography angiography in choroidal melanoma: an analysis of 22 consecutive cases. Retina. 2019;39:1510–9.
14. Valverde-Megías A, Say EA, Ferenczy SR, Shields CL. Differential macular features on optical coherence tomography angiography in eyes with choroidal nevus and melanoma. Retina. 2017;37:731–40.
15. Takkar B, Azad S, Shakrawal J, Gaur N, Venkatesh P. Blood flow pattern in a choroidal hemangioma imaged on swept-source-optical coherence tomography angiography. Indian J Ophthalmol. 2017;65:1240–2.
16. Konana VK, Shanmugam PM, Ramanjulu R, Mishra KCD, Sagar P. Optical coherence tomography angiography features of choroidal hemangioma. Indian J Ophthalmol. 2018;66:581–3.
17. Shields CL, Welch RJ, Malik K, Acaba-Berrocal LA, Selzer EB, Newman JH, et al. Uveal metastasis: clinical features and survival outcome of 2214 tumours in 1111 patients based on primary tumor origin. Middle East Afr J Ophthalmol. 2018;25:81–90.
18. Chen FK, Viljoen RD, Bukowska DM. Classification of image artefacts in optical coherence tomography angiography of the choroid in macular diseases. Clin Exp Ophthalmol. 2016;44: 388–99.
19. Kita Y, Holló G, Murai A, Kita R, Hirakata A. Optical coherence tomography angiography findings of an optic disc melanocytoma in a glaucoma eye. Int Ophthalmol. 2019;39:677–82.
20. Carnevali A, Querques L, Zucchiatti I, Scorcia V, Bandello F, Querques G. Optical coherence tomography angiography features in melanocytoma of the optic nerve. Ophthalmic Surg Lasers Imaging Retina. 2017;48:364–6.
21. Takkar B, Molla K, Venkatesh P. Swept-source optical coherence tomography of an optic disc melanocytoma: The importance of the hyperreflective foci. Indian J Ophthalmol. 2018;66:140–2.
22. Jain A, MB T, Shetty BK. Swept source optical coherence tomography angiography in optic disc melanocytoma. Can J Ophthalmol. 2018;53:e239–41.
23. Pichi F, Massaro D, Serafino M, Carrai P, Giuliari GP, Shields CL, et al. Retinal astrocytic hamartoma: optical coherence tomography classification and correlation with tuberous sclerosis complex. Retina. 2016;36:1199–208.
24. Mellen PL, Sioufi K, Shields JA, Shields CL. Invisible, honeycomb-like, cavitary retinal astrocytic hamartoma. Retinal Cases Brief Rep. 2020;14:211–4.

25. Yung M, Iafe N, Sarraf D. Optical coherence tomography angiography of a retinal astrocytic hamartoma. Can J Ophthalmol. 2016;5:e62–4.
26. Shanmugam PM, Konana VK, Ramanjulu R, Mishra KCD, Sagar P, Simakurthy S. Ocular coherence tomography angiography features of congenital hypertrophy of retinal pigment epithelium. Indian J Ophthalmol. 2019;67:563–6.
27. Falavarjani KG, Al-Sheikh M, Akil H, Sadda SR. Image artefacts in swept-source optical coherence tomography angiography. Br J Ophthalmol. 2017;101:564–8.
28. Naseripour M, Ghasemi Falavarjani K, Mirshahi R, Sedaghat A. Optical coherence tomography angiography (OCTA) applications in ocular oncology. Eye. 2020. https://doi.org/10.1038/s41433-020-0819-y.